Removal of Metal−Metal Bonding in a Dimetallic Paddlewheel Complex: Molecular and Electronic Structure of Bis(phenyl) Dirhodium(III) Carboxamidate Compounds

Joffrey Wolf,[†] Rinaldo Poli,*[,†,§] Jian-Hua Xie,[‡] Jason Nichols,[‡] Bin Xi,[⊥] Peter Zavalij,[‡] and Michael P. Doyle*[,‡]

Department of Chemistry and Biochemistry, University of Maryland, College Park, Maryland 20742, Laboratoire de Chimie de Coordination, UPR CNRS 8241 Liée par Convention à l'Université Paul Sabatier et à l'Institut National Polytechnique de Toulouse, 205 Route de Narbonne, 31077 Toulouse Cedex 4, France, Institut Universitaire de France, 103, Boulevard Saint-Michel, 75005 Paris, France, and Department of Chemistry, Purdue University, West Lafayette, Indiana 47907

Received July 5, 2008

The unique structural features and chemical stabilities of bis(phenyl) tetracarboxamidatodirhodium(III) are reported, and their electronic structures are mapped through XPS, electrochemical, and computational methods. Comparison with the structures of dirhodium(II,II) and dirhodium(II,III) oxidative precursors portrays the diphenyl dirhodium(III) compounds as two square-pyramidal rhodium units that have undergone conrotatory motion in order to optimize metal−ligand bonding. Axial phenyl ligands are severely distorted from their expected Rh−Rh−C linear array. XPS data for this series of dirhodium compounds are consistent with the absence of a rhodium−rhodium bond for the diphenyl dirhodium(III) compounds, and electrochemical measurement shows a single reversible Rh_2^{6+}/Rh_2^{7+} redox couple. Notably, they exhibit high thermal stability, and Brønsted acid removal of carboxamidate ligands precedes the formation of benzene. The ability of a phenyl group to impart unusual stability to rhodium(III) compounds is explained by theoretical analysis of the electronic structure of bis-σ-(phenyl)-tetrakis-μ-(carboxamido)dirhodium(III), and comparison is made with previously reported dinitrosyl dirhodium(III) complexes. Formally, two phenyl radicals in combination with a rhodium−rhodium bond are transformed into two phenyl−rhodium bonds. The severe distortion of phenyl rings from linearity is suggested to result from a long-range interaction between the electron-deficient rhodium and distal oxygen atoms.

Introduction

The recent definitive treatise on multiple bonds between metal atoms introduced oxidation states with the statement that "the most common oxidation states for the M_2^{n+} units in paddlewheel complexes correspond to values of n of 4, 5, and 6".[1] Examples of the $n = 6$ systems are less common. Our report last year of remarkably stable bis(phenyl)dirhodium(III) caprolactamate (Scheme 1, left)[2] was only the second example of Rh_2^{6+} compounds, the previously reported $Rh_2(O_2CR)_4(NO)_4$ (R = Me, Et, *i*Pr) (Scheme 1, center) exhibiting the same structural type and an essentially identical Rh−Rh separation.[3] Although no specific oxidation state assignment was mentioned in the Lippard report, the bent geometry observed for the NO ligands justifies the assignment of a formal oxidation state of III to the Rh centers, and this was later supported by computational studies.[4−6] One of the surprising features of these Rh_2^{6+} compounds is the apparent absence of a rhodium−rhodium bond. In contrast, a paramagnetic paddlewheel Ir_2^{6+} compound, $Ir_2(hpp)_4Cl_2$ (Scheme 1, right), also from group 9, has been reported to have a doubly bonded dimetallic core with two unpaired electrons.[7] Isoelectronic Ru_2^{4+} complexes are reported to have the $\sigma^2\pi^4\delta^2\delta^{*2}\pi^{*2}$ electronic configuration,[1,8] implying a Ru−Ru double bond and a spin triplet ground state, whereas Ru_2^{6+} compounds have the $\pi^4\delta^2\pi^{*4}$ electronic configuration with a net δ single bond.[1,9,10]

Homodinuclear σ-alkynyl complexes of both ruthenium and rhodium are known,[11] although with rhodium only in the (II,III) oxidation state.[12] Electron donation from the axial carbon ligand to rhodium increases the Rh−Rh bond distance, but only by a fraction of the lengthening found with **1**, and their electronic properties imply retention of a metal−metal bond.

The ability of paddlewheel complexes to hold together two metals without a metal−metal bond is well-established,[13,14] and

* Corresponding author. E-mail: rinaldo.poli@lcc-toulouse.fr.
[†] Université Paul Sabatier et Institut National Polytechnique de Toulouse.
[§] Institut Universitaire de France.
[‡] University of Maryland.
[⊥] Purdue University.

(1) Cotton, F. A.; Murillo, C. A.; Walton, R. A. *Multiple Bonds Between Metal Atoms*, 3rd ed.; Springer Science: New York, 2005.
(2) Nichols, J. M.; Wolf, J.; Zavalij, P.; Varughese, B.; Doyle, M. P. *J. Am. Chem. Soc.* **2007**, *129*, 3504–3505.
(3) Hilderbrand, S. A.; Lim, M. H.; Lippard, S. J. *J. Am. Chem. Soc.* **2004**, *126*, 4972–4978.
(4) Sizova, O. V. *J. Mol. Struct. (THEOCHEM)* **2006**, *760*, 183–187.
(5) Sizova, O. V.; Skripnikov, L. V.; Sokolov, A. Y.; Ivanova, N. V. *Russ. J. Coord. Chem.* **2007**, *33*, 588–593.
(6) Sizova, O. V.; Sokolov, A. Y.; Skripnikov, L. V.; Baranovski, V. I. *Polyhedron* **2007**, *26*, 4680–4690.
(7) Cotton, F. A.; Murillo, C. A.; Timmons, D. J. *Chem. Commun.* **1999**, 1427–1428.
(8) Cotton, F. A.; Ren, T.; Eglin, J. L. *Inorg. Chem.* **1991**, *30*, 2552–2558.
(9) Ren, T. *Organometallics* **2002**, *21*, 732–738.
(10) Bear, J. L.; Li, Y. L.; Han, B. C.; Kadish, K. M. *Inorg. Chem.* **1996**, *35*, 1395–1398.
(11) Hurst, S. K.; Ren, T. *J. Organomet. Chem.* **2003**, *670*, 188–197.
(12) Yao, C. L.; Park, K. H.; Khokhar, A. R.; Jun, M. J.; Bear, J. L. *Inorg. Chem.* **1990**, *29*, 4033–4039.

10.1021/om800631b CCC: $40.75
Publication on Web 10/22/2008

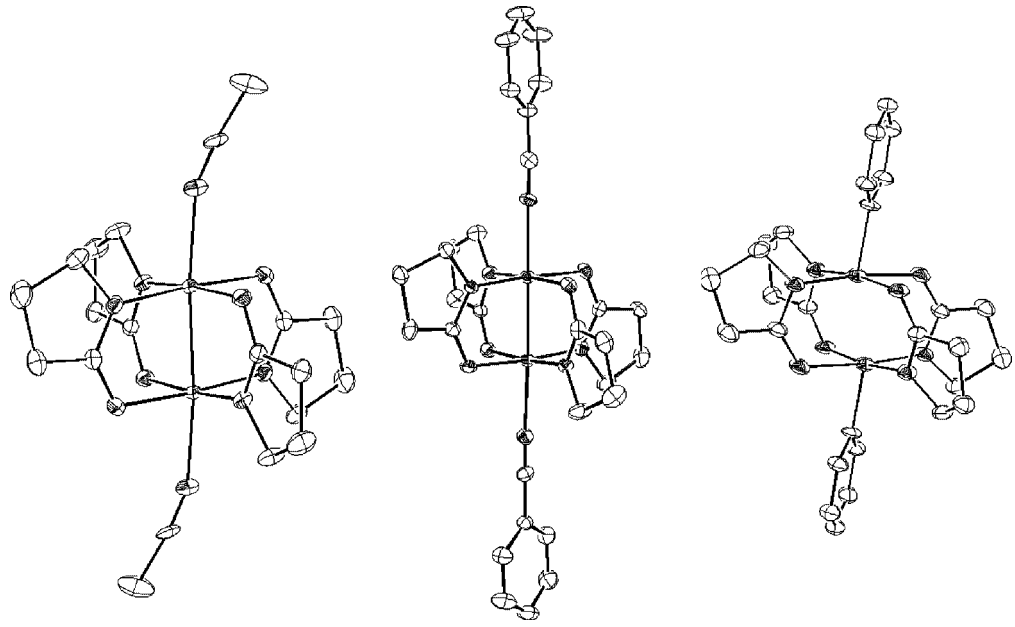

Figure 1. Structures of dirhodium pyrrolidinates (a) **1a**, (b) **2a′**, and (c) **3a**. Ellipsoids are shown at the 30% probability level. Hydrogen atoms, BF_4^- (for **2a′**), and solvent molecules are omited for clarity.

Scheme 1. Comparison of Two Isoelectronic Group 9 Paddlewheel Dimers

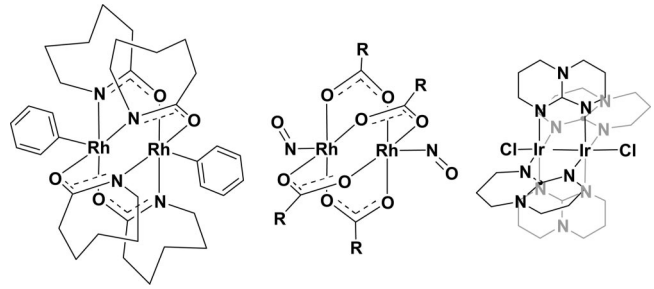

the structural and electronic influences that result have substantial theoretical and practical implications.[15] In this contribution, we report the molecular structures and chemical stabilities of the diphenyl tetracarboxamidatodirhodium(III) system and their study by XPS spectroscopy, electrochemistry, and computational methods.

Results and Discussion

Synthesis and Characterization. In order to identify the unique structural features of bis(phenyl)dirhodium(III) carboxamidates, we have prepared the dirhodium(II) pyrrolidinate (pyr), valerolactamate (val), and caprolactamate (cap) bis-acetonitrile complexes (**1**),[16] oxidized these compounds to the corresponding paramagnetic Rh(II)Rh(III) derivatives (**2**, eq 1), and also prepared their diamagnetic bis(phenyl)dirhodium(III) analogues (**3**, eq 2). The synthesis of dirhodium(II,III) complexes was achieved by oxidation of the dirhodium(II) carboxamidate using copper(II) triflate, nitrosonium salts (eq 1),[17,18] or phenyldiazonium tetrafluoroborate; oxidations with nitrosonium salts were the most versatile and gave dirhodium(II,III) product without byproducts in solution. As mentioned in the Introduction, the synthesis (using sodium tetraphenylborate) and characterization of bis(phenyl)dirhodium(III) caprolactamate (**3c**) has been described in a preliminary communication.[2] Since this first report, a new methodology for convenient access to diaryl analogues directly from dirhodium(II) carboxamidates and arylboronic acids catalyzed by copper sulfate (eq 2) has been communicated,[19] and the spectral data of these products have been described.

The crystal structures of all nine compounds have been obtained. Those of the pyrrolidinate systems $Rh_2(pyr)_4(MeCN)_2$ (**1a**), $[Rh_2(pyr)_4(PhCN)_2]BF_4$ (**2a′**), and $PhRh(pyr)_4RhPh$ (**3a**) are presented in Figure 1. Unpublished data for the other six compounds are provided as Supporting Information. A selection of bond lengths and angles for all nine compounds is reported in Tables 1 and 2. As can be seen from these data, the diphenyldirhodium(III) compounds exhibit severe structural distortions relative to their dirhodium(II,II) and dirhodium(II,III) analogues. They can best be evaluated by comparing a few key bond angles [the values are averages over the three structures within each family and listed in the order **1**, **2**, **3**]: L_{axial}−Rh−Rh [175(2)°, 174(4)°, 159(4)°]; Rh−O−C [118(2)°, 118(2)°, 126(1)°];

(13) Mendiratta, A.; Cummins, C. C.; Cotton, F. A.; Ibragimov, S. A.; Murillo, C. A.; Villagran, D. *Inorg. Chem.* **2006**, *45*, 4328–4330.
(14) Aakeroy, C. B.; Schultheiss, N.; Desper, J. *Dalton Trans.* **2006**, 1627–1635.
(15) Liu, C. S.; Wang, J. J.; Yan, L. F.; Chang, Z.; Bu, X. H.; Sanudo, E. C.; Ribas, J. *Inorg. Chem.* **2007**, *46*, 6299–6310.
(16) $Rh_2(pyr)_4(Hpyr)_2$ and $Rh_2(val)_4(Hval)_2$ have been prepared and their crystal structures reported: Bear, J. L.; Lifsey, R. S.; Chau, K. L.; Ahsan, M. Q.; Korp, J. D.; Chavan, M.; Kadish, K. M. *J. Chem. Soc., Dalton Trans.* **1989**, *9*, 3–100.
(17) Wang, Y.; Wolf, J.; Zavalij, P.; Doyle, M. P. *Angew. Chem., Int. Ed.* **2008**, *47*, 1439–1442.
(18) For uses of nitrosonium salts as oxidants, see: Connelly, N. G.; Geiger, W. E. *Chem. Rev.* **1996**, *96*, 877–910.
(19) Xie, J.-H.; Nichols, J. M.; Lubek, C.; Doyle, M. P. *Chem. Commun.* **2008**, 2671–2673.

Table 1. Selected Bond Lengths of Dirhodium Carboxamidates in the (II,II), (II,III), and (III,III) Oxidation States

		bond lengths of dirhodium complexes, Å		
	bond	**1a**	**2a′**[a]	**3a**
from $Rh_2(pyr)_4$	Rh1−Rh2	2.4540(5)	2.4432(4)	2.5738(12)
	Rh2−O1	2.077(2)	2.030(6)	2.093(6)
	Rh2−O2	2.080(2)	2.034(5)	2.095(5)
	Rh1−N1	2.003(3)	1.973(6)	1.993(7)
	Rh1−N2	2.011(3)	1.994(8)	2.012(6)
	Rh-L_{ax}	2.241(2)	2.248(8)	2.037(7)
	bond	**1b**	**2b′**[b]	**3b**
from $Rh_2(val)_4$	Rh1−Rh2	2.4187(5)	2.3872(3)	2.5162(5)
	Rh2−O1	2.061(2)	2.0143(16)	2.105(3)
	Rh2−O2	2.073(2)	2.0211(16)	2.061(2)
	Rh1−N1	2.023(3)	2.0078(19)	1.997(3)
	Rh1−N2	2.034(3)	2.016(2)	2.027(3)
	Rh−L_{ax}	2.254(3)	2.3071(16)	1.996(3)
	bond	**1c**	**2c**	**3c**
from $Rh_2(cap)_4$	Rh1−Rh2	2.4221(4)	2.3840(6)	2.5188(3)
	Rh2−O1	2.050(2)	2.023(2)	2.0825(16)
	Rh2−O2	2.053(2)	2.030(2)	2.0777(16)
	Rh1−N1	2.038(3)	1.988(3)	2.012(2)
	Rh1−N2	2.045(3)	1.996(3)	2.0078(19)
	Rh−L_{axial}	2.336(3)	2.288(2)	2.010(2)

[a] The bis-benzonitrile complex was prepared after failed attempts to prepare the bis-acetonitrile complex. [b] The bis-aquo complex was formed and crystallized, even though reaction was performed in acetonitrile.

Table 2. Selected Bond Angles for Dirhodium Carboxamidates in the (II,II), (II,III), and (III,III) Oxidation States

		bond angles of dirhodium complexes, deg		
	angle	**1a**	**2a′**[a]	**3a**
from $Rh_2(pyr)_4$	Rh1−Rh2−O1	90.04(6)	89.66(16)	82.43(15)
	Rh1−Rh2−O2	90.01(6)	89.94(15)	83.87(14)
	Rh2−Rh1−N1	85.30(7)	85.9(2)	89.32(18)
	Rh2−Rh1−N2	85.35(7)	86.15(18)	90.61(18)
	Rh2−O1−C1	115.16(19)	115.8(5)	121.1(4)
	Rh2−O2−C2	115.9(2)	117.7(5)	122.4(5)
	Rh1−N1−C1	123.40(2)	122.4(5)	118.0(5)
	Rh1−N2−C2	124.00(2)	123.7(5)	118.5(5)
	Rh1−Rh2−L_{axial}	176.90(7)	178.22(16)	164.20(20)
	angle	**1b**	**2b′**[b]	**3b**
from $Rh_2(val)_4$	Rh1−Rh2−O1	88.03(7)	89.61(5)	74.58(7)
	Rh1−Rh2−O2	88.85(7)	89.66(4)	85.05(7)
	Rh2−Rh1−N1	87.08(8)	87.11(5)	99.10(8)
	Rh2−Rh1−N2	87.89(8)	87.23(5)	88.47(8)
	Rh2- O1−C1	118.8(2)	118.89(14)	133.0(2)
	Rh2−O2−C2	119.3(2)	119.08(14)	122.1(2)
	Rh1−N1−C1	121.5(2)	121.10(16)	121.8(4)
	Rh1−N2−C2	121.8(2)	122.07(16)	119.8(2)
	Rh1−Rh2−L_{axial}	173.84(8)	172.27(5)	157.34(11)
	angle	**1c**	**2c**	**3c**
from $Rh_2(cap)_4$	Rh1−Rh2−O1	89.62(6)	88.58(7)	79.29(4)
	Rh1−Rh2−O2	89.37(6)	88.50(7)	78.39(5)
	Rh2−Rh1−N1	86.70(7)	88.42(8)	94.46(5)
	Rh2−Rh1−N2	86.81(7)	88.60(8)	95.32(5)
	Rh2−O1−C1	118.3(2)	119.8(2)	128.11(15)
	Rh2−O2−C2	118.96(19)	119.5(2)	128.97(15)
	Rh1−N1−C1	121.5(2)	120.8(2)	114.45(16)
	Rh1−N2−C2	121.7(2)	121.2(2)	113.51(15)
	Rh1−Rh2−L_{axial}	174.42(7)	171.28(7)	156.19(7)

[a] The bis-benzonitrile complex was prepared after failed attempts to prepare the bis-acetonitrile complex. [b] The bis-aquo complex was formed and crystallized, even though reaction was performed in acetonitrile.

Rh−N−C [122(1)°, 122(1)°, 118(1)°]. These distortions take the form of severe bending of the Rh−Rh−Ph bond axis from 180°, a major opening of the Rh−O−C angle, and a less pronounced closing of the Rh−N−C angle from the ideal 120°. The positioning of the rhodium units in the diphenyl-dirhodium structures appears as if two square-pyramidal units have undergone conrotatory motion so as to minimize repulsions and metal−metal interactions (Figure 2). In addition to these

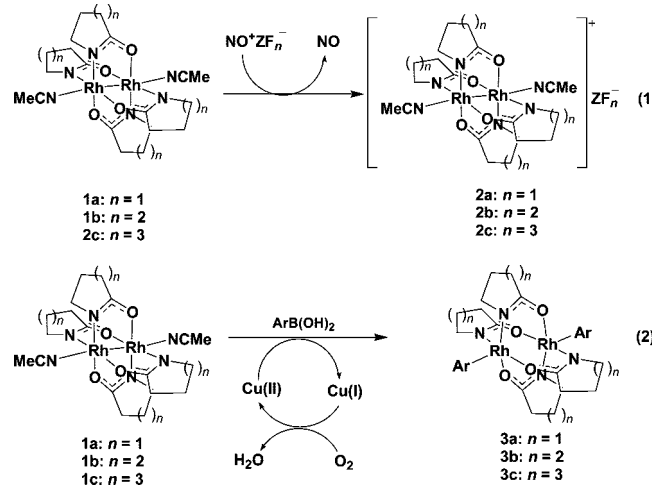

geometrical distortions, there is a significant lengthening of the Rh−Rh bond on going from **2** to **3**, whereas the bond shortens on going from **1** to **2**.

X-ray photoelectron spectroscopy (XPS) data for these nine compounds are given in Table 3. As evidenced by this direct measurement of the binding energy of d-electrons that constitute the dirhodium core, there is a significant change in binding energy upon oxidation of dirhodium(II,II) to dirhodium(II,III) (∼0.8 eV) but an insignificant change upon oxidation of dirhodium(II,III) to dirhodium(III,III) (<0.2 eV).

The relative electron richness of the diphenyldirhodium(III) carboxamidate complexes is also suggested by the results of an electrochemical investigation. Cyclic (CV) and differential pulse (DPV) voltammograms of **3a**, **3b**, and **3c** were measured in CH_2Cl_2, and their half-wave potentials ($E_{1/2}$) are reported in Table 4, along with their electronic absorption maxima (λ_{max}). Figure 3 shows the CV and DPV traces for $PhRh(pyr)_4RhPh$ (**3a**). For each of the complexes, a single, reversible Rh_2^{6+}/Rh_2^{7+} redox couple (A) was observed. The oxidation potential of **3** increases with decreasing number of methylene units in the bridging cyclic amide, which follows that of the $Rh_2^{4+/5+}$ couple of the parent complexes.[20] For complex **3a**, an additional irreversible redox couple (B) near the reduction limit of the solvent was observed and is assigned to the $Rh_2^{5+/6+}$ redox couple. Attempts to isolate and characterize the oxidized $PhRh(pyr)_4RhPh$ or any of its derivatives have thus far been unsuccessful.

The stabilities of bis(phenyl)dirhodium(III) carboxamidates are noteworthy. They are air stable and thermally stable to temperatures below 130 °C. They do not react with nucleophiles such as cyanide or azide, but they are sensitive to electrophilic attack. Treatment of compound bis-σ-(6-methoxynaphthalen-2-yl)-tetrakis-μ-(caprolactamato)dirhodium(II)[19] with trifluoroacetic acid, for example, resulted in quantitative conversion to 2-methoxynaphthalene (eq 3) and caprolactam (capH). Product analysis as a function of time with bis-σ-(phenyl)-tetrakis-μ-(caprolactamato)dirhodium(III) demonstrated the stability of the phenyl−rhodium(III) bond (Figure 4); caprolactam was released from the complex prior to release of benzene, but attempts to isolate the anticipated diphenyl derivative of dirhodium(III) trifluoroacetate were unsuccessful. Although bis-σ-(phenyl)-tetrakis-μ-(caprolactamato)dirhodium(III) was stable as a solid to temperatures above 200 °C with a measured decomposition point at 256 °C, when this compound was heated in refluxing chlorobenzene over long periods of time, biphenyl as well as mono-

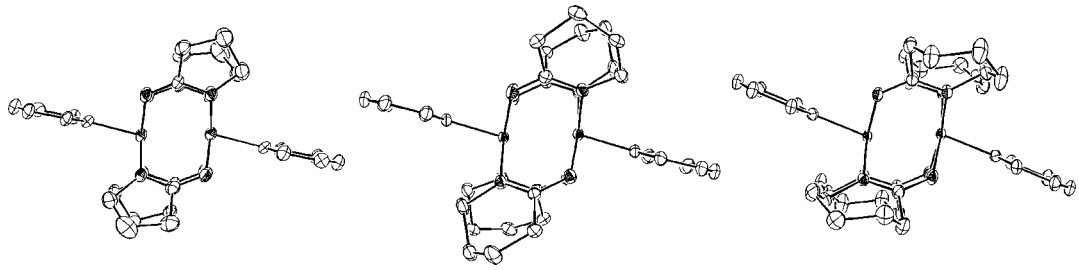

Figure 2. ORTEP views of (a) PhRh(pyr)$_4$RhPh (**3a**), (b) PhRh(val)$_4$RhPh (**3b**), and (c) PhRh(cap)$_4$RhPh (**3c**) showing comparable structural distortions. Ellipsoids are shown at the 30% probability level. Hydrogen atoms and solvent molecules are omitted for clarity. The corresponding Rh−Rh−C bond angles are 164.2° (**3a**), 157.3° (**3b**), and 156.2° (**3c**).

Table 3. XPS Data for Dirhodium Carboxamidates in the (II,II), (II,III), and (III,III) Oxidation States[a]

compound	Rh-3d$_{5/2}$, eV	Rh-3d$_{3/2}$, eV
Rh$_2$(pyr)$_4$(MeCN)$_2$ (**1a**)	308.000	312.563
Rh$_2$(val)$_4$(MeCN)$_2$ (**1b**)	308.129	312.843
Rh$_2$(cap)$_4$(MeCN)$_2$ (**1c**)	308.080	312.812
Rh$_2$(pyr)$_4$(PhCN)$_2$BF$_4$ (**2a′**)	308.905	313.514
Rh$_2$(val)$_4$(H$_2$O)$_2$BF$_4$ (**2b′**)	308.841	313.567
Rh$_2$(cap)$_4$(MeCN)$_2$BF$_4$ (**2c**)	309.094	313.718
PhRh(pyr)$_4$RhPh (**3a**)	309.045	313.739
PhRh(val)$_4$RhPh (**3b**)	309.011	313.723
PhRh(cap)$_4$RhPh (**3c**)	309.105	313.725

[a] Calibrated to carbon 1s at 284.6 eV.

Table 4. Electrode Potentials (V) from CV Measurements and λ_{max} of 3

compound	A (V)[a]	B (V)[b]	λ_{max} (nm)[c]
3a	0.91	−1.36	442
3b	0.81		429
3c	0.78		430

[a] Reversible anodic wave reported as $E_{1/2}$, measured with platinum wire/glassy carbon working electrodes against a Ag/AgCl reference electrode in CH_2Cl_2 with tetra-*n*-butylammonium hexafluorophosphate as the supporting electrolyte. [b] Irreversible cathodic reduction reported as cathodic peak potential (E_{pc}) in parentheses. [c] Measured in CH_2Cl_2.

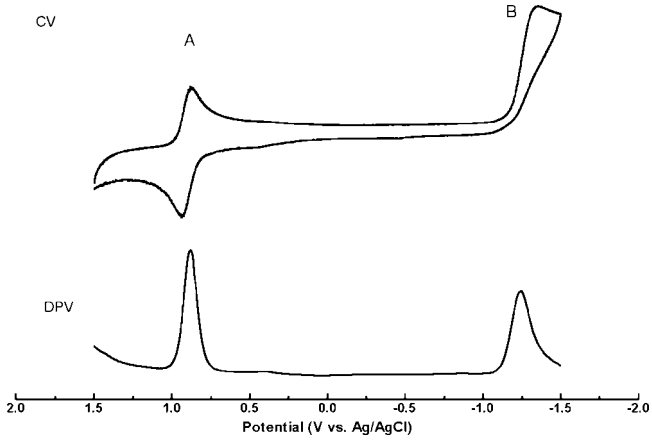

Figure 3. Cyclic (CV) and differential pulse voltammetry (DPV) measurements of **3a** recorded in 0.2 M CH_2Cl_2 solution of Bu_4NPF_6 at a scan rate of 0.10 V/s.

and dichlorobiphenyl are formed, suggestive of homolytic cleavage of the rhodium−phenyl bond.

Computational Study. The structural novelty of the bis(aryl)dirhodium(III) family and their peculiar properties (metal−metal bond length, stability) in comparison with isoelectronic systems (see Introduction) warrant a more detailed analysis of their electronic structure. DFT methods have proven quite successful when applied to dinuclear metal−metal bonded

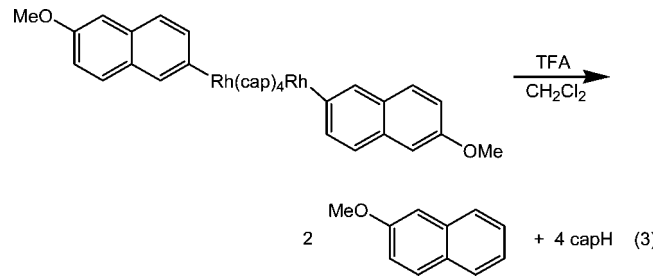

compounds.[21,22] The B3LYP functional provides the best agreement between experimental and calculated structures,[1] and it has therefore been adopted in this study. The study used the standard LANL2DZ basis set in order to provide a qualitative description of the electronic structure. A model system was constructed with the amidato ligands being replaced with simple formamidato ligands, [OCCHNH]$^-$.

(a) [Rh$_2$(amidato)$_4$], [Rh$_2$(amidato)$_4$(MeCN)$_2$], and [Rh$_2$(amidato)$_4$(MeCN)$_2$]$^+$ Systems. Before analyzing the more interesting bis(aryl)dirhodium(III,III) derivatives, it is necessary to start with the dirhodium(II,II) and dirhodium(II,III) precursors. These families of compounds have already been extensively studied; thus our analysis is limited to a comparison of the optimized and experimental geometries and to a comparison of the basic electronic structural features with those previously presented for other members of the same families[23−30] (fuller details are available as Supporting Information). Geometry optimizations were carried out for the simple tetrakis(amidato)dirhodium(II,II) system (**I** in Scheme 2), for its bis(acetonitrile) adduct (**II**), and for the one-electron oxidation product of the latter (**III**). All these calculations were carried out only with the experimentally observed head-head-tail-tail (*cis*-2,2)[20] relative orientation of the four bridging amidato ligands (see Scheme 2). The salient features of the optimized geometries are shown in Table 5. There is excellent agreement between optimized and experimental parameters, attesting to the suitability of the computational

(20) Doyle, M. P.; Ren, T. *Prog. Inorg. Chem.* **2001**, *49*, 113–168.
(21) Cotton, F. A.; Feng, X. *J. Am. Chem. Soc.* **1997**, *119*, 7514–7520.
(22) Cotton, F. A.; Feng, X. J. *J. Am. Chem. Soc.* **1998**, *120*, 3387–3397.
(23) Norman, J. G., Jr.; Kolari, H. J. *J. Am. Chem. Soc.* **1978**, *100*, 791–799.
(24) Norman, J. G., Jr.; Renzoni, G. E.; Case, D. A. *J. Am. Chem. Soc.* **1979**, *101*, 5256–67.
(25) Bursten, B. E.; Cotton, F. A. *Inorg. Chem.* **1981**, *20*, 3042–8.
(26) Cotton, F. A.; Feng, X. J. *Inorg. Chem.* **1989**, *28*, 1180–1183.
(27) Kawamura, T.; Maeda, M.; Miyamoto, M.; Usami, H.; Imaeda, K.; Ebihara, M. *J. Am. Chem. Soc.* **1998**, *120*, 8136–8142.
(28) Mougenot, P.; Demuynck, J.; Benard, M. *Chem. Phys. Lett.* **1987**, *136*, 279–282.
(29) Nakatsuji, H.; Ushio, J.; Kanda, K.; Onishi, Y.; Kawamura, T.; Yonezawa, T. *Chem. Phys. Lett.* **1981**, *79*, 299–304.
(30) Nakatsuji, H.; Onishi, Y.; Ushio, J.; Yonezawa, T. *Inorg. Chem.* **1983**, *22*, 1623–1630.

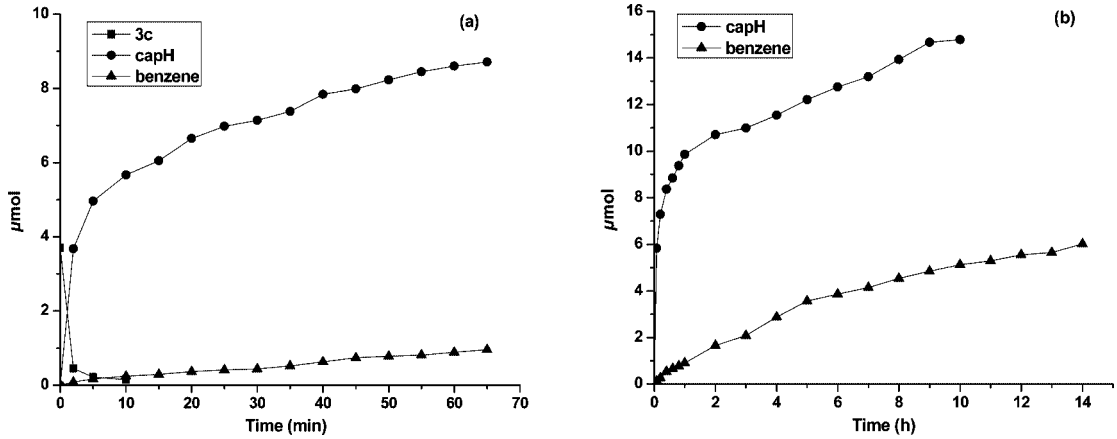

Figure 4. Reaction of PhRh(cap)$_4$RhPh (3.7 μmol) with (a) 10 and (b) 15 molar equiv of trifluoroacetic acid in $CDCl_3$ at room temperature.

Scheme 2. Tetraformamidato Systems Used for the DFT Calculations

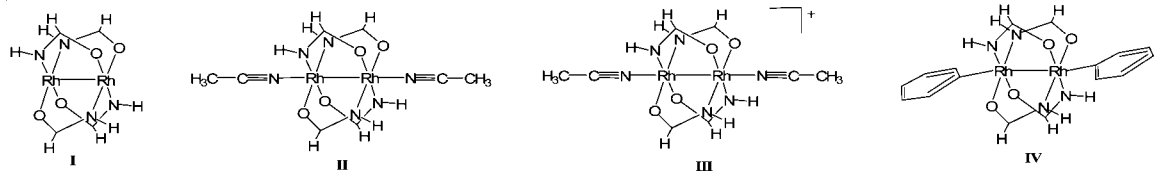

Table 5. Selected DFT-Optimized Geometric Parameters (distances in Å, angles in deg) for the Model Compounds I−III and Comparison with the Experimental Geometries

		system **II**		system **III**	
parameter	system **I**	opt	exptl[a]	opt	exptl[b]
(a) Distances					
Rh−Rh	2.454	2.497	2.43 (2)	2.481	2.40 (3)
Rh−N (amidato)	2.047	2.039	2.03 (2)	2.011	2.00 (2)
Rh−O	2.085	2.112	2.066 (4)	2.064	2.025 (7)
Rh−N(acetonitrile)		2.286	2.28 (5)	2.285	2.28 (3)
(b) Angles					
Rh−Rh−N (amidato)	87.15	86.36	87 (1)	86.95	87 (1)
Rh−Rh−O	89.25	88.80	89.3 (7)	88.32	89.3 (2)
Rh−Rh−N (acetonitrile)		176.61	175 (2)	177.54	174 (4)

[a] Averages over all chemically equivalent parameters of compounds **1a**, **1b**, and **1c**. [b] Averages over all chemically equivalent parameters of compounds **2a′**, **2b′**, and **2c**.

method and of the chosen model. The Rh−Rh distance trend is perfectly reproduced by the calculation. The very minor elongation (0.045 Å) computed on going from **I** to **II** agrees with the notion that this bond is rather insensitive to the presence of axial ligands, an experimental example being $Rh_2(O_2C-C_6H_2iPr_3$-2,4,6)$_4$ and its bis(acetone) adduct (distances of 2.350(1) and 2.370(1) Å, respectively).[31,32]

The specific Rh−Rh σ, π, and δ* interactions are symmetry-mixed with symmetry-adapted linear combinations (SALC) of the Rh−O and Rh−N bonds. The effect of this mixing is that each of these interactions is mainly distributed in two molecular orbitals. Within each pair of orbitals, the one carrying the greater Rh−Rh character is that at lower energy for σ and π and that at higher energy for δ*. From the energetic point of view, the major Rh−Rh σ MO is found at higher energy than the major Rh−Rh π MO, and the major Rh−Rh δ* MO is higher than the Rh−Rh π* MO. Upon MeCN axial ligation, the σ competition between the Rh−NCMe and Rh−Rh interactions has the effect of raising the Rh−Rh σ level. Weak axial ligands (e.g., H_2O) establish weak interactions with the Rh atoms and weakly affect the Rh−Rh σ MO energy,[23] whereas stronger ligands (e.g., phosphines) have a more pronounced effect and greatly raise the energy of the Rh−Rh σ MO to the point that this may even become the HOMO.[25] In the present case, the interaction is relatively weak but sufficient to push the Rh−Rh σ MO higher than the Rh−Rh δ MO but lower than the Rh−Rh π* MOs. Upon MeCN ligation, the energy of all orbitals is raised by ca. 0.4 eV on average, reflecting the additional electron density provided to the Rh atoms by the axial ligands. On the other hand, upon one-electron oxidation, all orbitals drop by ca. 1.5 eV on average as a result of the increased effective positive charge, but the MO energy ordering remains approximately unchanged (the σ level remains between the δ and π* levels). For all three systems, the HOMO (doubly occupied for I and II, singly occupied for III) is the Rh−Rh δ* MO.

(b) [Rh$_2$(amidato)$_4$Ph$_2$] System. A geometry optimization was carried out on the model system $Rh_2(OCHNH)_4(C_6H_5)_2$ with the same (*cis*-2,2) arrangement as in the **I**−**III** congeners (**IV**, see Scheme 2). The input geometry was constructed directly from the experimentally observed geometry of compound **3c**. Since this geometry is very close to an ideal C_{2h} symmetry, that symmetry was imposed in the initial geometry optimization.

(31) Cotton, F. A.; Hillard, E. A.; Murillo, C. A. *J. Am. Chem. Soc.* **2002**, *124*, 5658–5660.

(32) Cotton, F. A.; Hillard, E. A.; Liu, C. Y.; Murillo, C. A.; Wang, W. N.; Wang, X. P. *Inorg. Chim. Acta* **2002**, *337*, 233–246.

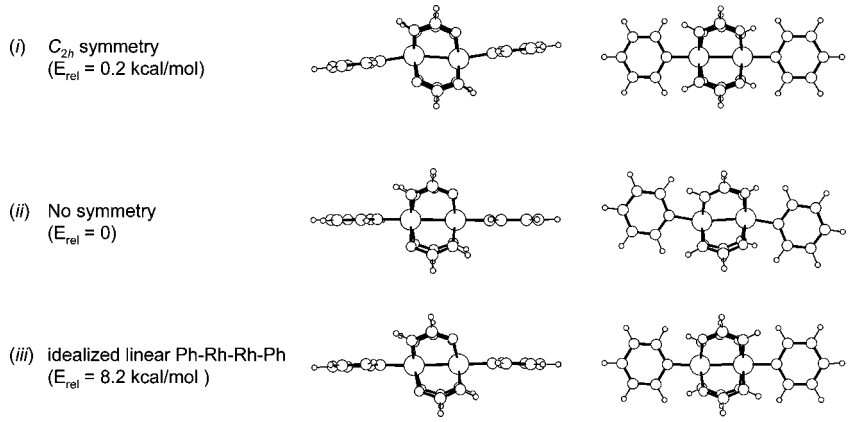

Figure 5. Two mutually perpendicular views of the geometries, and relative energies, of system **IV** obtained under three different conditions: (*i*) constrained optimization in C_{2h} symmetry; (*ii*) full optimization without symmetry constraints; (*iii*) idealized geometry with linear Ph−Rh−Rh−Ph moiety.

Table 6. Selected DFT-Optimized Geometric Parameters (distances in Å, angles in deg) for the Model Compound IV and Comparison with the Experimental Geometries

parameter	system IV (no symmetry)	system IV (C_{2h} symmetry)	expt[a]
(a) Distances			
Rh−Rh	2.644	2.639	2.54 (3)
Rh−N	2.025, 2.053	2.022	2.01 (2)
Rh−O	2.095, 2.133	2.138	2.09 (2)
Rh−C	1.999	1.999	2.01 (2)
(b) Angles			
Rh−Rh−N	90.22, 81.83	90.73	93 (1)
Rh−Rh−O	89.75, 81.50	81.13	81 (1)
Rh−Rh−C	166.92	166.44	159 (4)

[a] Averages over all chemically equivalent parameters of compounds **3a**, **3b**, and **3c**.

The converged geometry (Figure 5, *i*) remained very close to the initial one, but the frequency analysis revealed one imaginary frequency whose motion showed the tendency for the two Rh−Ph axes to move in opposite directions away from the symmetry plane. Therefore, a free optimization in C_1 symmetry was subsequently carried out. The resulting geometry (Figure 5, *ii*) was essentially C_i-symmetric, with the expected 3N-6 positive vibrational frequencies, and with a coplanar arrangement for the two Ph groups. The energy of the global minimum is just 0.2 kcal/mol lower than the C_{2h} structure. The ideal geometry where the Ph−Rh−Rh−Ph moiety was forced to be coplanar and linear (Figure 5, *iii*), on the other hand, turned out to be energetically less favored by 8.2 kcal/mol. These combined results indicate that the origin of the experimentally observed distortion of the Rh−Ph bonds is not in the steric interaction between the Ph groups and the amidato ligands, but rather in an electronic effect that forces the three-bond Ph−Rh−Rh−Ph sequence out of colinearity. Of the two different and nearly isoenergetic distortion modes (*i*) and (*ii*), the first one is adopted in the crystal structure for possible packing reasons.

Selected optimized geometric parameters for system **IV** are shown in Table 6. Like for systems **II** and **III**, the optimized structure of **IV** (C_{2h} symmetry) agrees very well with the observed structures. Except for the Rh−Rh distance (ca. 0.1 Å longer in the optimized geometry), all distances are in very close agreement with the experimentally determined structure. A significant difference is observed in the Rh−Rh−Ph angle (ca. 10° smaller in the X-ray structures), presumably because of crystal-packing effects. The distortion in the lower-energy C_i structure is different. It causes a slight asymmetry in the Rh

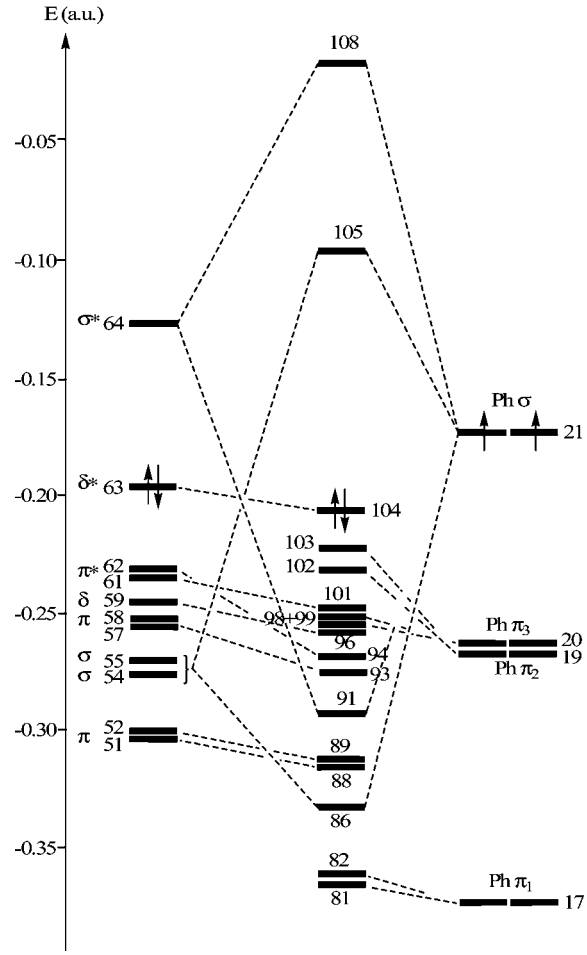

Figure 6. Simplified interaction diagram for system **IV**, built from the $Rh_2(OCHNH)_4$ fragment (**V**) and two phenyl radicals.

coordination geometry, yielding alternating long−short Rh−N and Rh−O distances. The longer distances are associated with the smaller Rh−Rh−X (X = N, O) angles.

The electronic structure analysis helps rationalize the molecular constitution and geometry of the novel dinuclear Rh^{III} complexes. The essential features are reported in Figure 6, while fuller details are presented in the Supporting Information. The relevant MOs for **IV** derive from the full geometry optimization, while those of the $Rh_2(OCHNH)_4$ fragment (**V**) and the Ph radicals are calculated for the corresponding fixed geometries

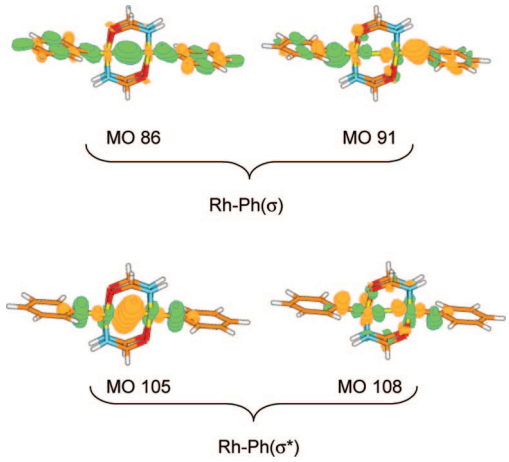

Figure 7. MOLDEN contour plots of relevant orbitals for system **IV**.

as found in **IV**. The frontier orbitals of interest for the Ph radical are the filled, familiar Huckel-type π_1, π_2, and π_3 orbitals, plus the σ orbital pointing out from the unsaturated carbon in a radial direction. The latter is expected to be used for the formation of the Rh^{III}−Ph σ bond.

Upon interaction between **V** and the two Ph radicals, we observe that those molecular orbitals that are not involved in a significant interaction change their energy only slightly. More specifically, there is a slight energy increase for the phenyl orbitals 17 (π_1) and 20 (π_3) and a slight energy decrease for **V** orbitals 51 and 52 (Rh−Rh π), 59 (Rh−Rh δ), and 63 (Rh−Rh δ*). Inspection of the contour plots of the related orbitals in system **IV** (see Supporting Information) shows that they do not involve a significant mixing of components from the different fragments.

The greater energy change experienced by the Ph π_2 orbitals is caused by the combination with the appropriately oriented Rh−Rh π and π* orbitals of **V**, resulting in Rh−Ph π-type interaction. However, since these are filled−filled interactions (both the in-phase and out-of-phase combinations are filled), there is no net Rh−Ph π bonding. The interaction is stronger (greater mixing and energy changes) for the Rh−Rh π* orbital because of a better energy match. The in-phase and out-of-phase combinations are found in orbitals 94 and 103, while the corresponding combinations with the Rh−Rh π MO are found in orbitals 93 and 102.

The most important interaction between **V** and the two Ph radicals results from the combination of the σ-type orbitals. There are four such orbitals in the frontier region, two for $Rh_2(OCHNH)_4$ (the filled Rh−Rh σ orbital, mixed with a nonbonding ligand-based combination in MOs 54 and 55, *vide supra*, and the empty Rh−Rh σ* orbital, MO 64) and two for the two Ph radicals (the half-filled frontier σ orbital, MO 21). This gives rise to two filled MOs (86 and 91) and to two empty MOs (105 and 108) in **IV**, all of which are shown in Figure 7 (a more extensive sample of MO contour diagrams for **IV** is presented in the Supporting Information). The two filled orbitals have mostly Rh−Ph σ character but also feature other contributions: the former has substantial Rh−Rh and C−C/C−H σ contributions, whereas the latter has Rh−Rh σ* character. Thus, very little Rh−Rh σ bonding is present in the molecule. Most of the Rh−Rh σ interaction is found in the empty MO 105, which also has significant Rh−Ph σ* character and is therefore raised above the energy of the Rh−Rh δ* orbital. Finally, MO 108 has both Rh−Rh and Rh−Ph σ* character (Figure 7). The Rh−Rh interaction in this molecule can therefore be formally described as $\pi^4\delta^2\pi^{*4}\delta^{*2}$, leading to a formal bond order of zero.

Using a basic, qualitative valence bond approach, we can describe the molecule as two interpenetrating octahedra, using the familiar d^2sp^3 hybrids for bonding. This would lead to the establishment of all three σ interactions (two Rh−Ph bonds and the Rh−Rh bond) by implication of the higher energy 5s and $5p_z$ orbitals for the two rhodium atoms. Obviously, this implication is not extensive enough to keep the third bonding orbital sufficiently low in energy to be occupied. We note that the involvement of the higher energy s orbital has been invoked[33] to rationalize the observed short distance of paddlewheel d^3−d^3 $W_2(O_2CEt)_4R'_2$ compounds (E = Et and R′ = CH_2Ph or CH_2tBu),[34] which are able to maintain their W−W σ interaction as in the parent d^4−d^4 $W_2(O_2CEt)_4$ compound. The involvement of the higher energy orbitals seems a more common feature for 5d elements, as a result of relativistic effects. The effect of the σ interaction scheme on the electronic structure is such that the HOMO of **IV** is the same orbital, the δ* orbital, as the HOMO of **I**. The two are essentially identical because the Ph groups do not significantly contribute. This agrees with the observed reversible electrochemical behavior upon oxidation: the electron is pulled off the essentially nonbonding δ* orbital; thus the Rh_2^{7+} oxidation product is predicted to have essentially no Rh−Rh bonding interaction and to display a structure closely related to that of its Rh_2^{6+} precursor.

One remaining point of interest is the origin of the nonlinear arrangement of the Ph−Rh−Rh−Ph moiety. One possible cause, related to the Ph−Rh−Rh−Ph σ bonding scheme, is a second-order Jahn−Teller effect involving the filled Rh−Ph and the empty Rh−Rh σ orbitals. However, this idea is contradicted by the higher energy of the bonding orbitals 86 and 91 in the optimized minimum relative to the idealized linear geometry (*iii* in Figure 5, orbital energies available in the Supporting Information). This suggests that the Ph−Rh−Rh−Ph σ-bonding framework prefers the linear configuration. The relative weakness of this interaction and its symmetry-mixing with other bonding features, however, do not allow its clear identification in the molecular orbitals. Therefore, the reason for the molecular distortion of **3** out of linearity must be attributed to other factors. A possible clue comes from the observation of very narrow Rh−Rh′−O bond angles in **3** (less than 90°), suggesting the presence of an attractive interaction between Rh and the O atom bonded to Rh′. The through-space crystallographic distances between rhodium and its distal oxygens are 3.00 and 3.24 Å for **3a**, 2.82 and 3.11 Å for **3b**, and 2.90 and 2.97 Å for **3c**. Given the absence of direct Rh−Rh bonding, the Rh atoms are in fact electronically unsaturated (16-electron configuration) and therefore seek electron density from the distal O lone pairs. However, we note that an alkylrhodium(III) compound with a nearly identical coordination geometry, the O_2N_2 coordination environment being provided by a Schiff base ligand, maintains a mononuclear five-coordination geometry with an open coordination site.[35]

(c) $[Rh_2(O_2CCH_3)_4(NO)_2]$ System. Compounds $Rh_2(O_2CR)_4(NO)_2$ (R = Me, Et, *i*Pr), featuring the same paddlewheel structure as compounds **3** with axial NO ligation and a very similar Rh−Rh distance, have been recently described.[3] The

(33) Chisholm, M. H.; Clark, D. L.; Huffman, J. C.; Van Der Sluys, W. G.; Kober, E. M.; Lichtenberger, D. L.; Bursten, B. E. *J. Am. Chem. Soc.* **1987**, *109*, 6796–6816.
(34) Chisholm, M. H.; Hoffman, D. M.; Huffman, J. C.; Vandersluys, W. G.; Russo, S. *J. Am. Chem. Soc.* **1984**, *106*, 5386–5388.
(35) Anderson, D. J.; Eisenberg, R. *Inorg. Chem.* **1994**, *33*, 5378–5379.

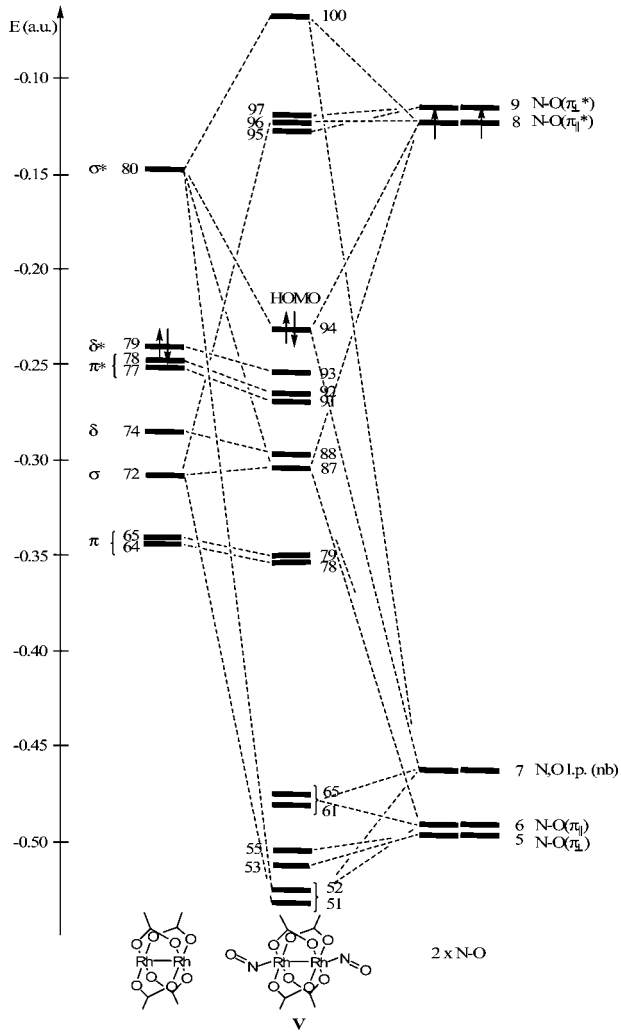

Figure 8. Simplified interaction diagram for system **VI**, built from $Rh_2(O_2CCH_3)_4$ and two nitrosyl radicals.

electronic structure of these compounds (with R = H and CH_3) has also been reported.[4−6] Here, we wish to compare the electronic structures of the system $Rh_2(O_2CCH_3)_4$-(NO) (**VI**) and **IV**. For this purpose, the geometry of **VI** has been optimized at the same computational level as **IV**. The orbital interaction diagram for **VI** with respect to its parent $Rh_2(O_2CCH_3)_4$ and NO fragments is shown in Figure 8, while fuller details of the electronic structure of **VI** are presented in the Supporting Information.

The axial donor, in this case, mostly interacts with the dimetal system via the N lone pair (which is mixed with the O lone pair in MO 7). However, because of the Rh−N−O bending, the NO $\pi_{||}$ and $\pi_{||}$* orbitals can also contribute to the Rh−Rh and Rh−N σ-bonding scheme. The perpendicular N−O π orbitals ($\pi_\perp$ and $\pi_\perp$*) have the correct symmetry to mix with the Rh−Rh π and π* components of the $Rh_2(O_2CCH_3)_4$ fragment, much like what happens in structure **IV** for the phenyl π_2 orbitals (*vide supra*).

Going from the fragments to the full system, as with the formamidato system discussed above, the metal−metal π, δ, π*, and δ* orbitals are not significantly affected. The N−O $\pi_\perp$ orbitals can potentially establish Rh−N π interactions but, because of their relatively deep energy, do not significantly mix with the metal orbitals and therefore are also little effected by the axial coordination. As for the amidato system, the most important change concerns the σ-type orbitals. Relative to the

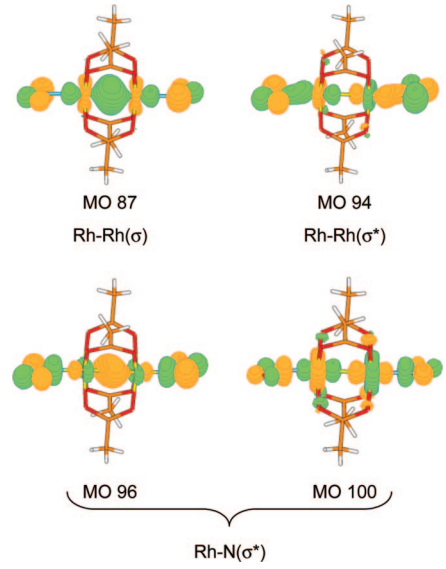

Figure 9. Contour plots of relevant orbitals for system **VI**.

diphenyl system, the situation is complicated by the greater number of participating orbitals [the Rh−Rh σ and σ* orbitals from fragment **V**, plus the N lone pair and the N−O $\pi_{||}$ and $\pi_{||}$* orbitals from each of the two NO ligands, for a total of eight resulting MOs]. The four lowest energy combinations (orbitals 51, 52, 61, and 65 in Figure 8) have their major contribution from the Rh−N σ and N−O $\pi_{||}$ bonds. Contour diagrams of the other four orbitals are shown in Figure 9 (other relevant orbitals are shown in the Supporting Information). They are qualitatively similar to those of system **IV**, including their occupation. Thus, as with the diphenyl formamidato system, the formation of the two Rh−NO bonds essentially destroys the Rh−Rh interaction, since the Rh−Rh σ* component that was empty in the dinuclear Rh^{II} fragment becomes now engaged in the axial σ-bonding system. That there is no N−Rh−Rh−N distortion in the nitrosyl complex is likely due to the symmetric nature of the three-atom bridges; since oxygen atoms constitute both sides, the molecule remains symmetric.

(d) Comparison of Electronic Structures. A comparison between the two MO diagrams of **IV** in Figure 6 and **VI** in Figure 8 shows that those orbitals with the largest Rh contribution, and not involved in the σ interactions (namely the π, π*, δ, and δ* orbitals), have lower energies for system **VI** than **IV**. This is rationalized by the more electronegative nature of the carboxylato ligands relative to the amidato ligands. The most important difference between the two systems, however, is in the σ manifold. For **IV**, the Rh−Rh(σ*) of the $Rh_2(OCHNH)_4$ fragment interacts strongly with the Ph donor orbitals, yielding a stabilized bonding orbital and leaving the Rh−Rh(δ*) orbital as the HOMO. The unexpectedly low observed increase in binding energy for the d electrons (XPS data in Table 3) upon going from compounds **2** to compounds **3** is consistent with the relatively small change of electronic structure in the frontier region and with the reversible oxidative electrochemistry (*vide supra*).

On the other hand, the interaction between the Rh−Rh(σ*) orbital of the $Rh_2(O_2CCH_3)_4$ fragment and the orbitals of the NO axial donors is not nearly as strong and yields a MO at relatively high energy, the HOMO of system **VI**. The nature of this orbital is Rh−Rh(σ*) and Rh−N(σ); see Figure 9, thus oxidation of this compound may be expected to lead to rupture of the Rh−NO interactions and to the establishment of a Rh−Rh bond. Thus, although systems **IV** and **VI** have a closely related

electronic structure and very similar bonding parameters, their chemical behavior toward oxidation should be drastically different.

It is also interesting to compare the electronic structure of these two systems with that of the isoelectronic Ir_2^{6+} complex $Ir_2(hpp)_4Cl_2$ (shown on the right in Scheme 1). No computational study on this system has been presented as yet, to the best of our knowledge. There is little doubt, however, that the general features of the electronic structure will parallel those presented above for systems **IV** and **VI**. The question of importance is the strength of the σ interaction between the axial ligands and the metal−metal framework. For the electronegative and spherically symmetrical Cl atom, the four resulting MOs (analogous to 86, 91, 105, and 108 for system **IV** or to 87, 94, 96, and 100 for system **VI**) would certainly end up at lower energy relative to the block of metal−metal orbitals of π and δ symmetry. The stronger relativistic effect for the 5d Ir element should also contribute to a stabilization of the orbitals of M−M σ symmetry through a greater involvement of the metal s orbital. In case the second highest of these four orbitals (having M−M σ and M−L_{ax} σ* contributions) is stabilized to the point of falling below the energy of the HOMO, then the molecule will indeed have a formal metal−metal double bond, because the two electrons needed to fill the M−M σ orbital originate from a previously filled antibonding orbital of π* or δ* type. If δ* is located below π*, the molecule will display two unpaired electrons, as is indeed observed for compound $Ir_2(hpp)_4Cl_2$.

Conclusion

The ability of a phenyl group to impart unusual stability to rhodium(III) compounds is explained by theoretical analysis of the electronic structure of bis-σ-(phenyl)-tetrakis-μ-(carboxamido)dirhodium(III). Formally, two phenyl radicals in combination with a rhodium−rhodium bond are transformed into two phenyl−rhodium bonds. The absence of a rhodium−rhodium σ-bonding interaction is suggested in the lengthening of the rhodium−rhodium distances from those of dirhodium(II,II) and dirhodium(II,III) complexes, as well as from XRD data and is confirmed by DFT analysis. The stability of the phenyl−rhodium bonds is seen in the preferential removal of equatorial carboxamidate ligands by trifluoroacetic acid and in the homolytic loss of phenyl radical from **3** at high reaction temperatures. The observed severe distortion of phenyl rings from linearity is suggested to have its origin in long-range interactions between the electron-deficient rhodium and the distal oxygen atoms. These structural characteristics are unique among M_2^{n+} compounds, and they suggest intriguing potential for future structural revelations.

Experimental Section

General Procedures. All oxidation reactions were performed in air. $NaBPh_4$ and CuOTf were purchased and used as received. ^{1}H NMR (400 MHz) and ^{13}C NMR (100 MHz) spectra were obtained from solutions in $CDCl_3$. Chemical shifts are reported in parts per million (ppm, δ) downfield from Me_4Si (TMS); coupling constants are reported in hertz (Hz). High-resolution mass spectra were done on an ESI instrument. UV−visible spectra were obtained using a xenon flash lamp. Both cyclic and differential pulse voltammograms were recorded in 0.2 M (n-Bu)$_4$NPF$_6$ solution (CH_2Cl_2, N_2-degassed) on a voltammetric analyzer with a glassy carbon working electrode, a platinum-wire auxiliary electrode, and a Ag/AgCl reference electrode. The ferrocenium/ferrocene couple was observed at 0.42 V (vs Ag/AgCl). All mass spectra were recorded on JEOL AccuTOF-CS from CH_2Cl_2 solution using MeCN/H_2O or MeOH/H_2O (9:1) as solvent in the presence of 1% triflic acid. Elemental analyses were carried out by the Service d'Analyse du Laboratoire de Chimie de Coordination in Toulouse. Dirhodium(II) acetate, carboxamidate ligands, and reagents described in this report were obtained commercially.

Tetrakis-μ-(pyrrolidinato)bis(acetonitrile)dirhodium(II) (1a).[16] In a dry flask under N_2 were mixed $Rh_2(OAc)_4$ (500 mg, 1.31 mmol), 2-pyrrolidinone (2.3 g, 27.0 mmol), and anhydrous chlorobenzene (40 mL). The flask was equipped with a Soxhlet apparatus with a thimble containing a 2:1 $NaHCO_3$/sand mixture (5 g). The solution was kept under N_2 and stirred at reflux for 24 h, after which the solution was cooled and solvent was removed under reduced pressure. The residue was washed with diethyl ether (2 × 50 mL) and pentane (50 mL). The purple solid obtained was heated at 80 °C in acetonitrile (15 mL), and some methanol was added to dissolve the entire solid. The mixture was crystallized at 20 °C to give a pink-red solid. Yield: 565 mg (80%). Suitable X-ray quality crystals (pink-red prisms) were obtained by slow evaporation of diethyl ether from an acetonitrile solution. ^{1}H NMR (400 MHz, CD_3CN + CD_3OD): δ 3.55 (br, N-CH_2), 3.44 (m, N-CH_2), 2.34 (t, ^3J = 7.6 Hz, 8H, $\underline{CH_2}$-C), 1.98 (q, ^3J = 7.6 Hz, 8H, N-CH_2-$\underline{CH_2}$). ^{13}C NMR (100 MHz, CD_3CN + CD_3OD): δ 186.89 (s, NCO), 55.41 (s, N-CH_2), 33.12 (s, $\underline{CH_2}$-C), 21.91 (s, N-CH_2-$\underline{CH_2}$). MS (ESI), m/z, (%): 584.01, (100) $[Rh_2C_{18}H_{28}N_5O_4]^+$ = M(MeCN)$^+$; 625.04, (28) $[Rh_2C_{20}H_{31}N_6O_4]$ = M(MeCN)$_2^+$. UV/visible spectrum (MeCN + MeOH, one drop), λ (ϵ, M^{-1} cm^{-1}): 350 nm (224); 505 nm (235). XPS: Rh-3d a 5/2 308.000 eV; Rh-3d b 5/2 309.082 eV; Rh-3d a 3/2 312.563 eV; Rh-3d b 3/2 313.648 eV.

Tetrakis-μ-(pyrrolidinato)bis(acetonitrile)dirhodium(II,III) Tetrafluoroborate (2a). A solution of $NOBF_4$ (22.3 mg, 191 μmol) in anhydrous acetonitrile (9 mL) was slowly added (over 3 min) to a suspension of **1a** (108.5 mg, 174 μmol) in CH_2Cl_2 (25 mL). The suspension rapidly turned from purple to dark red-purple. After complete addition the mixture was stirred for an additional 30 min at room temperature. Solvents were removed under reduced pressure, and the residue was dissolved in CH_2Cl_2 (5 mL), then filtered. The filtrate was concentrated (ca. 2−3 mL), precipitated in diethyl ether (50 mL), filtered, and dried under vacuum. A dark red-violet solid was obtained (117.2 mg, 94.8%), but the bis-acetonitrile complex did not form crystals suitable for X-ray analysis. Suitable X-ray crystals (black plate) of the bis(benzonitrile) adduct, **2a′**, were obtained after an axial ligand exchange (by heating the product 5 min at 60 °C in a small amount of benzonitrile) and a layer diffusion of diethyl ether in a 2:1 benzonitrile/CH_2Cl_2 solution. A satisfactory elemental analysis for this compound could not be obtained, presumably because of the facile axial ligand exchange. NMR silent; HRMS (ESI) calcd for $Rh_2C_{18}H_{27}N_5O_4$ (M(MeCN)$^+$) 583.01731, found 583.01516. MS (ESI), m/z, (%): 574.1, (100) $[Rh_2C_{17}H_{28}N_4O_5]^+$ = M(MeOH)$^+$; 542.0, (24) $[Rh_2C_{16}H_{24}N_4O_4]^+$ = M$^+$; 87.0, (100) $[BF_4]^-$. UV/visible spectrum (CH_2Cl_2), λ (ϵ, M^{-1} cm^{-1}): 489 nm (4150); 530 nm (−); 1030 nm (1440). XPS: Rh-3d a 5/2 308.905 eV; Rh-3d b 5/2 310.722 eV; Rh-3d a 3/2 313.514 eV; Rh-3d b 3/2 315.069 eV.

Bis-σ-(phenyl)-tetrakis-μ-(pyrrolidinato)dirhodium(III) (3a). To a MeOH/CH_2Cl_2 solution (5 mL, 1:1) of **2a** (30.5 mg, 42.9 μmol) were added $NaBPh_4$ (73.4 mg, 214.5 μmol) and CuOTf (1.5 mg, 7.1 μmol). The initial purple solution rapidly turned to yellow-green, and the mixture was stirred at room temperature for 18 h. During this period a yellow-green solid precipitated. Solvents were removed under reduced pressure, MeOH (10 mL) was added to the residue, and the mixture was stirred 5 min to obtain a homogeneous suspension. The mixture was filtered, washed with MeOH (2 × 5 mL) and Et_2O (10 mL), and dried under vacuum to give a yellow-green product. Yield: 20.6 mg (69%). Suitable crystals (yellow prism) for X-ray analysis were obtained by slow evaporation of dichloromethane from a CH_2Cl_2 solution. Anal. Calcd for $C_{28}H_{34}N_4O_4Rh_2$ (MW = 696.41): C 48.29, H 4.92, N 8.05. Found:

C 48.10, H 4.93, N 7.29. ^{1}H NMR (400 MHz, $CDCl_3$): δ 7.33 (m, 4H, *o*-Ph), 7.1 (m, 6H, *m,p*-Ph), 3.64 (m, 4H, N-CH_2), 3.01 (m, 4H, N-CH_2), 2.52 (m, 4H, CH_2−C), 2.41 (m, 4H, CH_2−C), 1.94 (m, 4H, N-CH_2-$\underline{CH_2}$), 1.82 (m, 4H, N-CH_2-$\underline{CH_2}$). ^{13}C NMR (100.6 MHz, $CDCl_3$): δ 183.00 (s, NCO), 141.18 (d, $^1J_{Rh-C}$ = 34 Hz),, 136.60 (s, *o*-Ph), 127.50 (s, *m*-Ph), 125.21 (s, *p*-Ph), 53.46 (s, N-CH_2), 34.12 (s, $\underline{CH_2}$-C), 21.82 (s, N-CH_2-$\underline{CH_2}$). UV/visible spectrum (CH_2Cl_2): 442 nm (ϵ = 4492 M^{-1} cm^{-1}). HRMS (ESI) calcd for $Rh_2C_{28}H_{35}N_4O_4$ 697.07684, found 697.07580 (MH^+). XPS: Rh-3d a 5/2: 309.045 eV; Rh-3d a 3/2: 313.739 eV.

Compounds 1b, 2b, 2b′, 3b, 1c, 2c, and 3c. These compounds were synthesized by the same general procedures described above for compounds **1a**, **2a**, **2a′**, and **3a**. The details are given as Supporting Information.

Reaction of Bis-σ-(6-methoxynaphthalen-2-yl)-tetrakis-μ-(caprolactamato)dirhodium(III) with Trifluoroacetic Acid. A solution of trifluoroacetic acid (114 mg, 1.0 mmol) in CH_2Cl_2 (1 mL) was slowly added (over 5 min) to a solution of bis-σ-(6-methoxynaphthalen-2-yl)-tetrakis-μ-(caprolactamato)dirhodium(II) (52 mg, 53.7 μmol) in anhydrous CH_2Cl_2 (6 mL). The reaction solution rapidly turned from green to orange. After the addition was complete, the mixture was stirred at room temperature for 24 h. Solvents were then removed under reduced pressure, and the residue was chromatographed on silica gel using hexanes/EtOAc (10:1) as eluent. The product, 2-methoxynaphthalene, was obtained as a white solid (15.5 mg, 91% yield). Mp: 71−73 °C; lit.[36] 71−73 °C. ^{1}H NMR (400 MHz, $CDCl_3$): δ 7.76−7.74 (m, 3H), 7.44−7.39 (m, 1H), 7.34−7.29 (m, 1H), 7.14−7.10 (m, 2H), 3.91 (s, 3H).

Reaction of 3c with Trifluoroacetic Acid. In a dry NMR tube were added 3.0 mg (3.7 μmol) of bis(phenyl)dirhodium(III) caprolactamate (**3c**) and 0.5 mL of $CDCl_3$. After the solid was dissolved and a clear green solution was obtained, 13 μL (18.5 μmol, 5 equiv), 26 μL (37.0 μmol, 10 equiv), or 39 μL (55.5 μmol, 15 equiv) of trifluoroacetic acid solution in $CDCl_3$ (1.35 mmol/mL) was then added. The mixture was rapidly oscillated for a minute and then submitted to ^{1}H NMR to follow reaction progress. Spectra were taken every 5 min for 1 h and then every hour, and data were obtained by using $CHCl_3$ in $CDCl_3$ as an internal standard.

Computational Details. All geometry optimizations were performed using the B3LYP three-parameter hybrid density functional method of Becke,[37] as implemented in the Gaussian03 suite of programs.[38] The basis functions consisted of the standard LANL2DZ for all atoms, which included the Hay and Wadt effective core potentials (ECP)[39] for Rh. Unless otherwise stated, the geometry optimizations were carried out without any symmetry constraint and the final geometries were characterized as local minima of the potential energy surface (PES) by verifying that all second derivatives of the energy were positive. The unrestricted formulation was used for the open-shell, mixed-valence Rh_2^{5+} system. The value of $\langle S^2 \rangle$ at convergence was 0.7579, very close to the expected value of 3/4, indicating minor spin contamination.

Acknowledgment. We are grateful to the National Science Foundation (CHE-0456911) for their generous support. We also thank the Fond Social Européen for funding J.W. and Bristol-Meyers-Squibb for supporting J.N. with an American Chemical Society Organic Division Fellowship. R.P. thanks the CICT (Project CALMIP) for granting free computer time.

Supporting Information Available: Synthesis and characterization of **2** and **3**. Crystallographic data for eight compounds (**1**−**3**) in CIF format are available. Cartesian coordinates and relative energies of all optimized structures. Energies, composition, and contour diagrams of the relevant molecular orbitals for geometry-optimized systems **I**, **II**, **III**, **IV**, and **VI**. This material is available free of charge via the Internet at http://pubs.acs.org.

OM800631B

(36) Arsenijevic, L.; Arsenijevic, V.; Horeau, A.; Jacques, J. *Org. Synth.* **1973**, *53*, 5–8.
(37) Becke, A. D. *J. Chem. Phys.* **1993**, *98*, 5648–5652.
(38) Frisch, M. J.; et al. *Gaussian 03, Revision B.04*; Gaussian, Inc.: Wallingford, CT, 2003.
(39) Hay, P. J.; Wadt, W. R. *J. Chem. Phys.* **1985**, *82*, 270–283.